

# Reduced-Rank STAP for High PRF Radar

T. F. AYOUB

A. M. HAIMOVICH, Senior Member, IEEE  
New Jersey Institute of Technology

M. L. PUGH  
USAF Rome Laboratory

Due to the range ambiguity of high pulse-repetition frequency (HPRF) radars, echoes from far-range fold over near-range returns. This effect may cause low Doppler targets to compete with near-range strong clutter. Another consequence of the range ambiguity is that the sample support for estimating the array covariance matrix is reduced, leading to degraded performance. It is shown that space-time adaptive processing (STAP) techniques are required to reject the clutter in HPRF radar. Four STAP methods are studied in the context of the HPRF radar problem: low rank approximation sample matrix inversion (SMI), diagonally loaded SMI, eigencanceler, and element-space post-Doppler. These three methods are evaluated in typical HPRF radar scenarios and for various training conditions, including when the target is present in the training data.

Manuscript received February 12, 1998; revised October 14, 1998.

IEEE Log No. T-AES/35/3/06413.

This work was supported in part by Air Force Rome Laboratory Grant F30602-94-1-0012.

Authors' current addresses: T. F. Ayoub and A. M. Haimovich, Dept. of Electrical and Computer Engineering, New Jersey Institute of Technology, 323 Martin Luther King Jr. Blvd., Newark, NJ 07102, E-mail: (haimovic@megahertz.njit.edu); M. L. Pugh, Air Force Research Laboratories/IFEA, 32 Brooks Rd., Rome, NY 13441-4114.

0018-9251/99/\$10.00 © 1999 IEEE

## I. INTRODUCTION

Radar returns often contain interference echoes from unwanted objects that can obscure echoes from targets of interest. In airborne radar, ground clutter returns from all ranges and all angles appear to be moving relative to the platform. These mainlobe and sidelobe clutter returns are spread over a region in Doppler given by  $\pm 2Vf_c/c$  Hz, where  $V$  is the platform velocity,  $f_c$  is the carrier frequency of the radar, and  $c$  is the speed of light. The geometry of a typical airborne radar scenario is shown in Fig. 1. The Doppler frequency associated with each clutter patch seen by the radar is given by  $f_d = (2V/\lambda)\sin\phi\cos\theta$ , where  $\lambda$  is the wavelength corresponding to the transmitted carrier frequency,  $\phi$  is the azimuth angle, and  $\theta$  is the depression angle. A target of interest may be masked by mainlobe clutter that originates at the same angle as the target or by sidelobe clutter that originates from different angles, but has the same Doppler frequency as the target. Effective suppression of these clutter returns, which extend in both angle and Doppler, requires spatial and temporal degrees of freedom.

For missions such as airborne early warning, radar systems may employ high pulse-repetition frequency (HPRF) waveforms to enhance long-range detection of high closing-rate targets that appear in the clutter-free region of the Doppler spectrum of the radar system. However, a basic limitation of the HPRF waveform is that due to range ambiguities, strong, near-range clutter returns received in the antenna sidelobes cannot be simply gated out and are, therefore, folded in with signal returns that fall within the Doppler bandwidth of the clutter. This can result in the masking of targets of interest at lower Doppler frequencies. Mitigation of these clutter returns using techniques such as space-time adaptive processing (STAP) would enhance the ability of HPRF radars to detect lower Doppler targets in clutter. In recent years, STAP has been studied and applied mainly to low pulse-repetition frequency (LPRF) radar problems [1-5]. The application of STAP to the HPRF radar problem presents a unique set of challenges different from traditional LPRF radar applications.

In this work, the issue of range-ambiguous sample support is addressed and several STAP methods is investigated for the HPRF radar. With traditional sample matrix inversion (SMI), the adaptive weight vector is computed from the inverse of the sample covariance matrix. In HPRF radar, the covariance matrix is likely to be singular as a result of reduced sample support. The performance is investigated using the pseudoinverse in lieu of the inverse covariance matrix. This method is referred to as *pseudoinverse sample matrix inversion* (P-SMI). The second method investigated is the diagonally

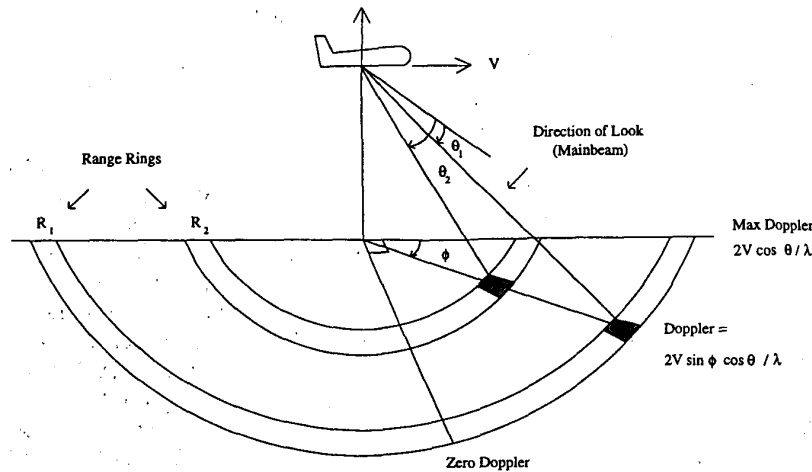


Fig. 1. Geometry of airborne radar problem.

loaded SMI (L-SMI) [6, 7]. This method is traced back to the early 1980s with publications translated from Russian [8, 9]. With L-SMI the singularity of the sample covariance matrix is overcome by diagonal loading. The last STAP technique investigated in this paper is the eigencanceller [10].

In general, the covariance matrix estimate used by the various STAP methods is obtained using target-free data. The presence of the target in the training data has two adverse effects: 1) it causes target cancellation in case of calibration errors [10], and 2) it causes further performance degradation due to covariance matrix estimation errors. The latter effect vanishes asymptotically as the number of samples increases. In HPRF radar, the sample support is limited and the target presence in the training data has a nonnegligible impact. L-SMI and the eigencanceller are members of the class of *reduced-rank* techniques. Such methods [10–12] have been shown to outperform full-rank methods such as SMI for limited sample support.

In this paper, the application of STAP to HPRF is evaluated through a number of performance measures such as output signal-to-clutter and noise ratio and probability of detection. Also investigated is the performance of an element space post-Doppler processor where Doppler filtering is applied prior to adaptive spatial processing to reduce the data dimensionality.

The organization of the paper is as follows. Section II presents the signal model, the problem associated with HPRF airborne radars and the suggested processing strategy; Section III discusses the STAP techniques and element-space post-Doppler and the performance measures used to compare them; numerical analysis is presented in Section IV and the conclusions in Section V.

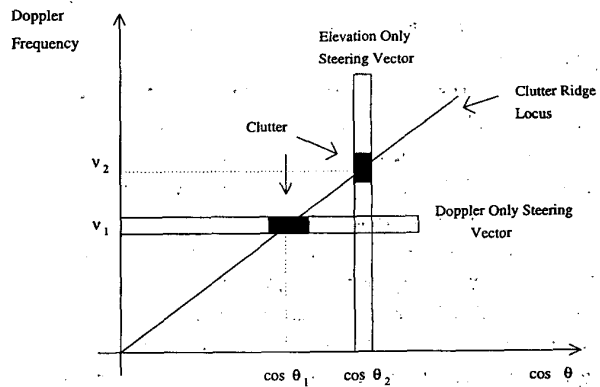


Fig. 2. STAP for HPRF radar.

## II. PROBLEM FORMULATION

Clutter seen by an airborne radar extends in both space and time domains. To reject this clutter, temporal and spatial degrees of freedom are needed. Elevation angle is a spatial variable of interest in the processing of HPRF radar returns because a target and clutter overlapping due to range ambiguity are not necessarily separated in azimuth angle, but can be usually discriminated in elevation angle. This observation is particularly true for mainlobe clutter. Clutter returns form a “ridge” in the Doppler-elevation ( $\nu - \theta$ ) plane. The ridge locus is given by  $\nu = k \cos \theta$ , where  $k = (2V/\lambda) \sin \phi$ . If only temporal (Doppler) processing is used, and the Doppler “mainbeam” points at frequency  $\nu_1$ , then the clutter at elevation angle  $\theta_1 = \cos^{-1}(\nu_1/k)$ , will compete with the target (see Fig. 2). Conversely, if only elevation processing is employed, and the mainbeam points to elevation angle  $\theta_2$ , then the clutter at Doppler frequency  $\nu_2 = k \cos \theta_2$  will compete with the target. The clutter ridge associated with the azimuth mainlobe can therefore be eliminated only by STAP.

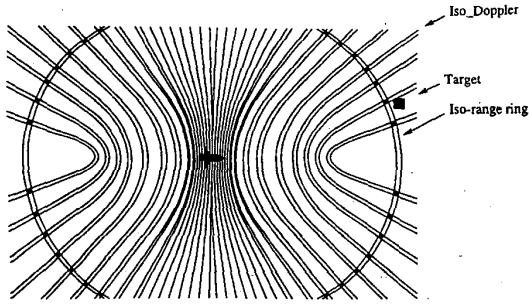


Fig. 3. Iso-Doppler, Iso-range ring map for LPRF radar.

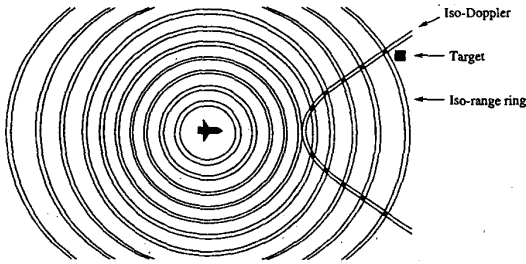


Fig. 4. Iso-Doppler, Iso-range ring map for HPRF radar.

As a result of the airborne radar platform's motion, regions of ground clutter may end up competing with targets of interest in both range and Doppler. Differences in the regions of competing clutter for LPRF and HPRF radar cases are illustrated in Figs. 3 and 4, respectively. As shown in Fig. 3, regions of competing clutter for LPRF airborne radars are located at the same range as the target on iso-Doppler contours, which are ambiguous with the target Doppler frequency. As shown in Fig. 4, regions of competing clutter for HPRF airborne radars are located at the same Doppler frequency as the target on iso-range rings, which are ambiguous with the target range. Due to range ambiguities, these regions of sidelobe clutter are folded in with mainbeam target returns and can be a significant source of interference, especially when they are located at relatively short ranges and steep grazing angles as illustrated in Fig. 5. Hence STAP techniques need to be implemented which allow cancellation of the near-range sidelobe clutter while protecting the target in the mainbeam. Mainbeam clutter will have a different Doppler frequency than a moving target and therefore can be rejected.

Consider a linear space-time array with  $N_s$  equally spaced antennas and a coherent pulse interval (CPI) consisting of  $N_t$  pulses. After carrier demodulation, matched filtering and sampling, the data received at the array is organized into the  $(N = N_s N_t)$ -dimensional vector  $\mathbf{x}_k$ , where the index represents an ambiguous range cell. The vector  $\mathbf{x}_k$  contains samples of the complex envelope of a bandpass signal and hence it is complex-valued. Under hypothesis  $\mathbf{H}_0$ , no signal is present and  $\mathbf{x}_k$  is the sum of clutter  $\mathbf{c}_k$  and additive

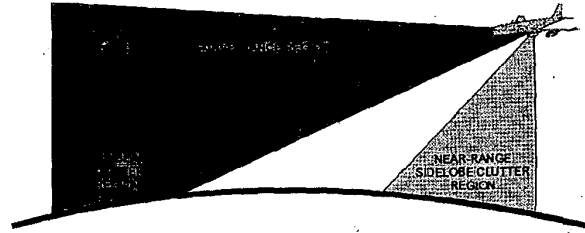


Fig. 5. Surveillance geometry.

white Gaussian noise contributions  $\mathbf{n}_k$ :

$$\mathbf{H}_0 : \mathbf{x}_k = \mathbf{c}_k + \mathbf{n}_k. \quad (1)$$

The clutter and noise are assumed to be independent. The signal model under  $\mathbf{H}_1$  is given by

$$\mathbf{H}_1 : \mathbf{x}_k = a\mathbf{s} + \mathbf{c}_k + \mathbf{n}_k \quad (2)$$

where  $a$  is a zero-mean, complex Gaussian random variable with variance  $\sigma_t^2$  and  $\mathbf{s}$  represents the space-time (S-T) steering vector defined as an  $(N = N_s N_t)$ -dimensional vector and is given by the Kronecker product of the spatial and temporal vectors

$$\mathbf{s} = \mathbf{s}_s \otimes \mathbf{s}_t \quad (3)$$

where  $\mathbf{s}_s = (1/\sqrt{N_s}) [1, \dots, e^{j2\pi(N_s-1)u_t}]^T$  is the normalized spatial steering vector,  $\mathbf{s}_t = (1/\sqrt{N_t}) [1, \dots, e^{j2\pi(N_t-1)v_t}]^T$  is the normalized temporal steering vector, the symbol  $\otimes$  denotes the Kronecker product,  $u_t$  and  $v_t$  are respectively the spatial and Doppler frequencies of the presumed target,  $u_t = d/\lambda \sin \phi_t \cos \theta_t$ , and  $v_t = 2V_t/\lambda \text{PRF}$ ,  $d$  is the spacing between the antenna elements,  $\phi_t$  is the azimuth angle of the target,  $\theta_t$  is the elevation angle of the target, and  $V_t$  is the velocity of the target relative to the platform. The unambiguous range of the radar is related to the pulse-repetition frequency (PRF) by  $R_{un} = c/(2\text{PRF})$ . If the range of the target extends beyond  $R_{un}$ , the target return is folded over near-range clutter echoes. Radar echoes will have an apparent range  $R_{app}$ , and a true range  $R_{true}$ , which are related by

$$R_{app} = R_{true} - R_{un} [R_{true}/R_{un}] \quad (4)$$

where the brackets denote integer part. Hence, the data vector  $\mathbf{x}_k$  consists of the sum of contributions of all the range cells folded onto the cell corresponding to index  $k$ . The number of data samples equals the number of range cells in the unambiguous range interval. Strictly speaking, range data samples will not be identically distributed since the radar cross section is a function of range as well as elevation angle. However, the clutter returns that dominate the covariance matrix are from near-range, close to Nadir. In this work, it is assumed that the range interval associated with the dominant clutter contributions is small and that the  $K$  data vectors representing the unambiguous range closest to the radar are

independently drawn from the same distribution. The maximum likelihood estimate of the covariance matrix is given by

$$\hat{\mathbf{R}} = \sum_{k=1}^K \mathbf{x}_k \mathbf{x}_k^H \quad (5)$$

Clearly, if  $K < N$ , the matrix is singular. The sample support size  $K$  is controlled by the radar's unambiguous range and range resolution. For low rank interference, the true covariance matrix  $\mathbf{R}$ , can be decomposed into interference and white noise contributions. Its spectral decomposition can be written as

$$\mathbf{R} = \mathbf{Q}_r \mathbf{\Lambda}_r \mathbf{Q}_r^H + \sigma_v^2 \mathbf{Q}_v \mathbf{Q}_v^H \quad (6)$$

where the diagonal of the  $r \times r$  matrix  $\mathbf{\Lambda}_r$  consists of the  $r$  principal eigenvalues of  $\mathbf{R}$ , the columns of  $\mathbf{Q}_r$  are the corresponding eigenvectors,  $\sigma_v^2$  is the variance of the white noise, and the columns of  $\mathbf{Q}_v$  are the remaining eigenvectors of  $\mathbf{R}$ . In practice, the noise-free covariance matrix will have all non-zero eigenvalues. However, for any system, the space-time array included, the rank of  $\mathbf{R}$  can be approximated by the Landau-Pollak relation [13]  $r \cong 2BT + 1$ , where  $B$  is the clutter bandwidth and  $T$  is the time a received signal dwells across the filter structure. The application of the Landau-Pollak relation to the space-time array is discussed in [4, 10]. The number of principal eigenvalues in a calibrated space-time array is upper bounded by

$$r \leq N_s + 2(N_t - 1)\nu_{\max} \quad (7)$$

where  $\nu_{\max} = 2V/(\lambda \text{PRF})$  is the highest normalized Doppler component of the clutter returns. In the HPRF radar case,  $\nu_{\max} \ll 1$  since the clutter occupies only a fraction of the Doppler spectrum. Thus, the HPRF problem is of lower rank than an equivalent LPRF problem. Effects of underestimating or overestimating the rank  $r$  were studied previously (see [14]) and are not considered here.

#### A. J-Hook Clutter

In an airborne HPRF application, clutter enters the receiver primarily through the mainbeam and principal elevation sidelobes. This is illustrated in the clutter intensity plot, shown in Fig. 6. The mainbeam of the radar is shown in the figure. It can be observed that at far-range, clutter returns are approximately parallel to the iso-Doppler contours. This implies little variation in the Doppler frequency. As it approaches Nadir, the clutter ridge traverses an increasing number of iso-Doppler contours. This results in the characteristic J-hook curvature of the clutter ridge in the range-Doppler domain shown in Fig. 7. As this plot illustrates, for the HPRF waveform, most of the Doppler band is clutter free. The range ambiguity is

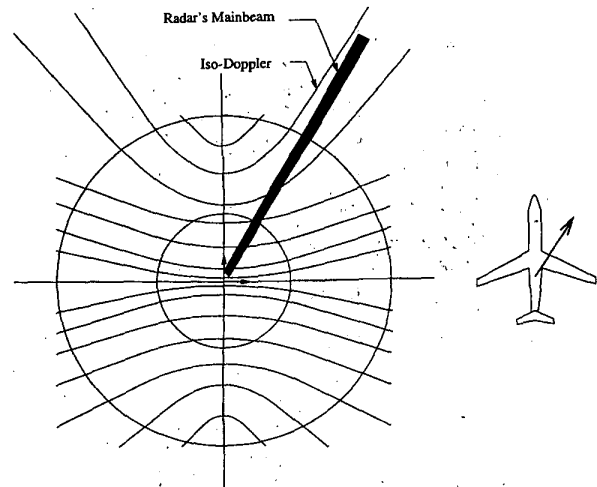


Fig. 6. HPRF clutter intensity map.

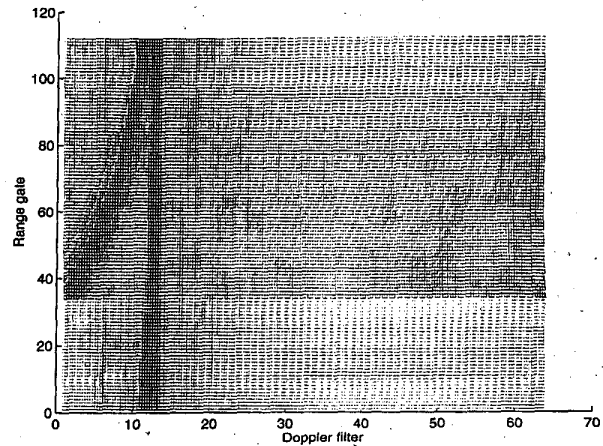


Fig. 7. Clutter map for HPRF radar.

demonstrated by clutter at different Dopplers having the same range. Far-range clutter has little Doppler variation and is shown as a vertical line. Near-range clutter crosses many iso-Dopplers and is shown as a J-shaped curve. Detection of fast-moving targets is accomplished in the clutter-free Doppler region. The problem is detection of a slow-moving target embedded in the J-hook clutter.

The formation of the J-hook characteristic can be shown also mathematically by analyzing the elevation angle-Doppler frequency relation. The Doppler frequency of the clutter is given by

$$f_d = (2V/\lambda) \sin \phi \cos \theta \quad (8)$$

The elevation angle  $\theta$  can be expressed in terms of the Doppler frequency as

$$\theta = \cos^{-1} \left( \frac{\lambda}{2V} \frac{f_d}{\sin \phi} \right) = \cos^{-1} (k_1 f_d) \quad (9)$$

where  $k_1$  is a constant. To relate range and Doppler frequency, note that  $R_{\text{true}} = H/\tan \theta$ , where  $H$  is

altitude. It follows that

$$R_{\text{true}} = \frac{H}{\tan(\cos^{-1}(k_1 f_d))}. \quad (10)$$

This expression plotted as a function of  $f_d$  results in the J-shaped curve.

### III. STAP FOR HPRF RADAR

Several STAP methods are compared by the *conditioned signal-to-noise ratio* (CSNR) and the probability of detection. The CSNR is defined as the ratio of the effective signal-to-noise ratio (SNR) obtained using the weight vector derived from the estimated covariance matrix using the respective STAP method, to the optimal SNR when the covariance matrix is known,

$$\text{CSNR} = \rho = \frac{\text{SNR}_{\text{eff}}}{\text{SNR}_{\text{opt}}} \quad (11)$$

where given the STAP weight vector  $\mathbf{w}$ ,  $\text{SNR}_{\text{eff}}$  is given by

$$\text{SNR}_{\text{eff}} = \frac{|\mathbf{w}^H \mathbf{s}|^2}{\mathbf{w}^H \mathbf{R} \mathbf{w}} \quad (12)$$

and the optimal SNR,  $\text{SNR}_{\text{opt}}$  is

$$\text{SNR}_{\text{opt}} = \mathbf{s}^H \mathbf{R}^{-1} \mathbf{s}. \quad (13)$$

The CSNR is a random variable bounded by  $0 \leq \rho \leq 1$ . Probability density functions for SMI, L-SMI, and eigencanceler, have been obtained, respectively, in [9, 10, 15].

The four methods evaluated for HPRF are P-SMI, L-SMI, eigencanceler, and element-space post-Doppler. These methods are briefly reviewed below.

The P-SMI method is defined when the estimated covariance matrix  $\hat{\mathbf{R}}$  is singular, and its inverse is replaced by the *pseudoinverse*. The pseudoinverse is given by

$$\hat{\mathbf{R}}_{\#} = (\hat{\mathbf{R}}_M^H \hat{\mathbf{R}}_M)^{-1} \hat{\mathbf{R}}_M^H \quad (14)$$

where  $\hat{\mathbf{R}}_M$  is the low-rank approximation to  $\hat{\mathbf{R}}$ . The matrix  $\hat{\mathbf{R}}_M$  is constructed from the singular value decomposition of  $\hat{\mathbf{R}}$  [16]:

$$\hat{\mathbf{R}}_M = [\mathbf{U}_1 \quad \mathbf{U}_2] \begin{bmatrix} \Sigma_M & \mathbf{0} \\ \mathbf{0} & \mathbf{0} \end{bmatrix} \begin{bmatrix} \mathbf{V}_1^H \\ \mathbf{V}_2^H \end{bmatrix} = \mathbf{U}_1 \Sigma_M \mathbf{V}_1^H \quad (15)$$

where  $\Sigma_M$  is the  $M \times M$  diagonal matrix of the  $M$  principal singular values of  $\hat{\mathbf{R}}$ . The two unitary matrices  $\mathbf{U}_1$  and  $\mathbf{V}_1$  are the left singular vectors and right singular vectors of  $\hat{\mathbf{R}}_M$ , respectively. The P-SMI weight vector is then given by

$$\mathbf{w} = \hat{\mathbf{R}}_{\#} \mathbf{s}. \quad (16)$$

The diagonally loaded SMI (L-SMI) is a modification of the traditional SMI method in which a constant is added to the diagonal of the estimated covariance matrix  $\hat{\mathbf{R}}$  in order to improve numerical conditioning. This constant is referred to as the loading factor. In [9] it is suggested that when the sample support  $K < N$ , the loading factor  $\alpha$  should be selected such that  $\sigma_v^2 < \alpha < \lambda_{\min}$ , where  $\lambda_{\min}$  denotes the smallest interference eigenvalue. The L-SMI weight vector is then given by

$$\mathbf{w} = (\hat{\mathbf{R}} + \alpha \mathbf{I})^{-1} \mathbf{s}. \quad (17)$$

The loading of the covariance matrix decreases the fluctuations of the small eigenvalues, which are predominantly noise eigenvalues, and as a result decreases fluctuations in  $\mathbf{w}$ .

For a loading factor  $\alpha$  within the allowable range, the distribution of the CSNR for L-SMI is given by [9]

$$f(\rho) = \frac{1}{B(K-r+1, r)} \rho^{K-r} (1-\rho)^{r-1} \quad (18)$$

where  $B(\cdot)$  is the beta function,  $K$  is the sample support, and  $r$  is the rank of the interference subspace.

The weight vector of the eigencanceler is given in [10] by

$$\mathbf{w} = (\mathbf{I} - \hat{\mathbf{Q}}_r \hat{\mathbf{Q}}_r^H) \mathbf{s} = \hat{\mathbf{Q}}_v \hat{\mathbf{Q}}_v^H \mathbf{s} \quad (19)$$

where  $\hat{\mathbf{Q}}_r$  and  $\hat{\mathbf{Q}}_v$  are approximations of  $\mathbf{Q}_r$  and  $\mathbf{Q}_v$ , respectively, in (6), and  $\mathbf{I}$  is the identity matrix. The asymptotic distribution of the CSNR for the eigencanceler was derived in [17]. It is shown that the CSNR  $\rho$  can be expressed as

$$\rho = \frac{1}{1 + \frac{1}{K} \zeta} \quad (20)$$

where  $\zeta = \sum_{i=1}^r \nu_i$ , and  $\nu_i$  are independent and identically distributed random variables with exponential distribution and hence,  $\zeta$  is a Gamma random variable with  $r$  degrees of freedom and parameter 1. This characterization results in the density

$$f(\rho) = K \rho^{-1} \sum_{i=1}^r \frac{\pi_i}{\bar{\nu}_i} \exp\left(\frac{-K \left(\frac{1}{\rho} - 1\right)}{\bar{\nu}_i}\right) \quad (21)$$

where  $\pi_i = \prod_{j=1, j \neq i}^r \bar{\nu}_j / (\bar{\nu}_j - \bar{\nu}_i)$ .

In [17], an approximation can be found to the pdf for large interference-to-noise ratio. This is given by

$$f(\rho) = \frac{K^r}{\Gamma(r)} e^{-K\rho} \rho^{r-1};$$

here  $\Gamma(\cdot)$  is the standard gamma function.

The element-space post-Doppler processor (terminology borrowed from [4]) performs Doppler processing on the data from each array element

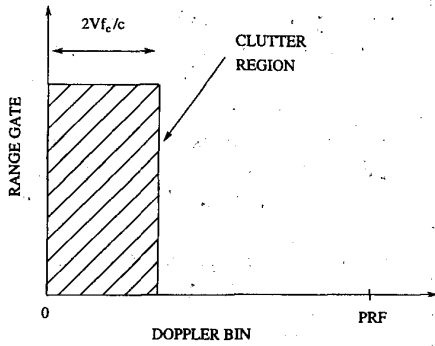


Fig. 8. Clutter region for HPRF radar.

prior to the adaptive array. Hence, the space-time data snapshot is transformed into a snapshot of the elements of the array at each Doppler bin. Thus, a different adaptive problem is solved in each Doppler bin. After Doppler filtering is applied to the space-time data, SMI can be used to calculate the adaptive weight vector as

$$\mathbf{w} = k \hat{\mathbf{R}}_s^{-1} \mathbf{s}_s \quad (22)$$

where  $\hat{\mathbf{R}}_s$  is the spatial covariance in the chosen Doppler bin,  $\mathbf{s}_s$  is the spatial steering vector, and  $k$  is a complex constant. The advantages of such an algorithm are summarized in the following.

- 1) Reduced data dimension provides improved conditioning of the covariance matrix.
- 2) There is a faster conversion rate (with respect to the number of samples required to estimate the covariance matrix), since the size of the matrix to be inverted is smaller.
- 3) This algorithm is suitable to apply to HPRF radar where the Doppler shifts of the clutter do not extend over the bandwidth of the entire radar. Hence, processing and detection needs to be applied only in a fraction of the total number of Doppler bins. This is illustrated in Fig. 8.

## B. Robustness Analysis

In Section II it was noted that HPRF radars employing adaptive arrays are typically faced with reduced sample support for training. The covariance matrix estimate given in (5) assumes target-free samples of the interference and noise. If the target is present in the training data, then performance might be adversely affected due to two main reasons: 1) mismatches between the target vector (as incorporated in  $\hat{\mathbf{R}}$ ) and the steering vector will result in signal cancellation, and 2) the presence of the target amplifies the effect of errors in the estimation of the covariance matrix. Mismatches between the actual target vector and the steering vector are the result of calibration errors. The steering vector is obtained

during the calibration phase of the system. In a perfectly calibrated system (target vector colinear with the steering vector), the presence of the target in the training data does not affect the system performance [18]. Calibration errors, however, translate into a target vector that is not colinear with the steering vector. In this case, we may regard the target vector to be the resultant of two vectors: one colinear with the steering vector and the other orthogonal to it. The orthogonal component is seen by the canceler as an interference. Subsequently, the system will act to reject it, resulting in some target cancellation. Target cancellation due to calibration errors is analyzed in more detail in [14].

In addition to the calibration errors, performance is affected by errors in the estimation of the covariance matrix. Due to the reduced sample support, range cells containing the target form a nonnegligible share of the overall number of snapshots available for training. The covariance matrix estimate in the presence of the target is

$$\hat{\mathbf{R}}_t = \hat{\mathbf{R}} + \sum_{k=1}^L |a_k|^2 \mathbf{s} \mathbf{s}^H \quad (23)$$

where  $\hat{\mathbf{R}}$  was defined in (5),  $L$  is the number of range cells containing the target, and  $|a_k|^2$  is the target power in a range cell. From (23) and (5), it can be seen that if  $K \gg L$ ,  $\hat{\mathbf{R}}_t \approx \hat{\mathbf{R}}$ . The CSNR in the presence of the target can be written

$$\rho_t = \frac{|\mathbf{w}_t^H \mathbf{s}|^2}{\mathbf{w}_t^H \hat{\mathbf{R}} \mathbf{w}_t \mathbf{s}^H \hat{\mathbf{R}}^{-1} \mathbf{s}} \quad (24)$$

where  $\mathbf{w}_t$  is the weight vector obtained using  $\hat{\mathbf{R}}_t$  rather than  $\hat{\mathbf{R}}$ . It is shown in [19] that the following relation exists between  $\rho$  and  $\rho_t$ :

$$\rho_t = \frac{\rho}{\text{SNR}_{\text{opt}}(1-\rho) + 1} \quad (25)$$

Since  $0 \leq \rho \leq 1$ , it is obvious that the CSNR with the target present is lower than when the training does not include the target,  $\rho_t \leq \rho$ . Equality holds only when  $\rho = 1$ , i.e., the true covariance matrix is available. A closed-form expression can be obtained for  $E[\rho_t]$  for L-SMI. It is not too difficult to show that

$$\begin{aligned} E[\rho_t] &= \int_0^1 \rho_t f(\rho_t) d\rho_t \\ &= \left( \frac{1+K-r}{1+K} \right) (1 + \text{SNR}_{\text{opt}})^{1+K-r} \\ &\quad \times {}_2F_1[1+K; 2+K-r; 2+K; -\text{SNR}_{\text{opt}}], \\ &\quad K > r-2 \end{aligned} \quad (26)$$

where  ${}_2F_1$  is a hypergeometric function [20]. The mean CSNR,  $E[\rho_t]$ , is a function of the desired signal

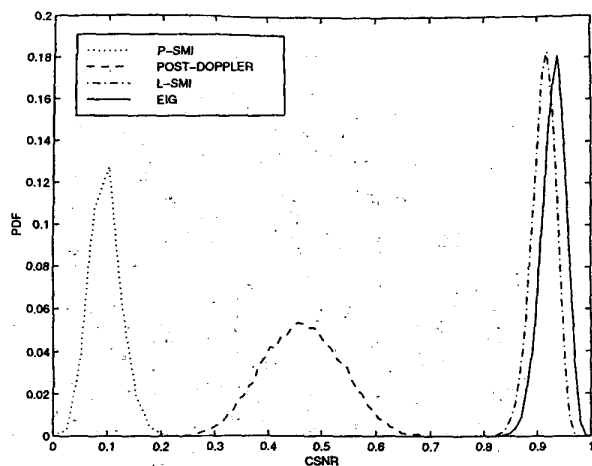


Fig. 9. PDF of CSNR.

power. The mean CSNR is inverse proportional to the target signal power. For a finite  $K$  and  $\text{SNR}_{\text{opt}} \rightarrow \infty$ ,  $E[\rho_r] \rightarrow 0$ .

#### IV. NUMERICAL RESULTS

The performance of the HPRF radar with STAP was investigated by simulations. The simulation model assumed a linear uniform antenna array with  $N_s = 8$  elements spaced at half wavelength. Each array channel consisted of a  $N_t = 64$  tap finite impulse response (FIR) filter. The system under consideration was assumed located on an airborne platform at an altitude of 30,000 ft, and moving with a constant velocity of 250 m/s. The clutter was assumed to come from all elevation angles and was modeled to have a complex-valued Gaussian distribution, with zero mean, and variance equal to a prescribed value of 60 dB clutter-to-noise ratio (CNR). It was further assumed that the clutter returns are uncorrelated with each other and also uncorrelated between snapshots. Attenuation due to free-space propagation was assumed proportional to  $R_{\text{true}}^{-3}$ , where  $R_{\text{true}}$  is the true range of the cell under test. The radar PRF was chosen to be 25 KHz. The transmitted frequency of the radar was 3.3 GHz. The target was placed at a range of 90 km and a Doppler frequency of  $0.05 \times \text{PRF}$ . The unambiguous range was calculated to be 6 km.

The sample covariance matrix was estimated from  $K = 112$  range cells. Equations (16), (17), (19), and (22) were used, respectively, to calculate the STAP weight vectors for P-SMI, L-SMI, eigencanceler, and element-space post-Doppler methods. After analyzing the data, the eigencanceler weight vector was computed based on an interference rank of  $r = 21$ . Densities of the CSNR for each of the methods were computed from 10,000 Monte-Carlo runs and

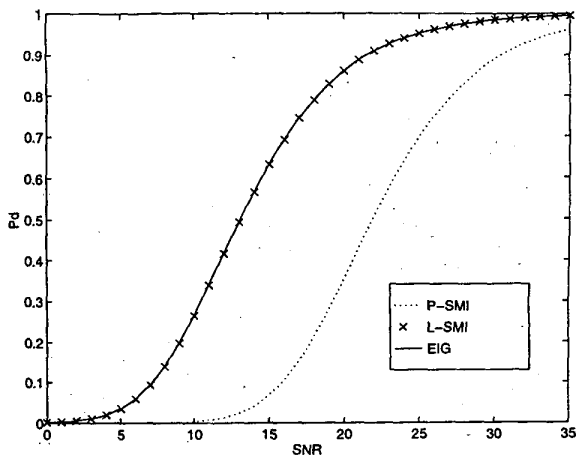


Fig. 10. Probability of detection of CSNR obtained by averaging 200 runs.

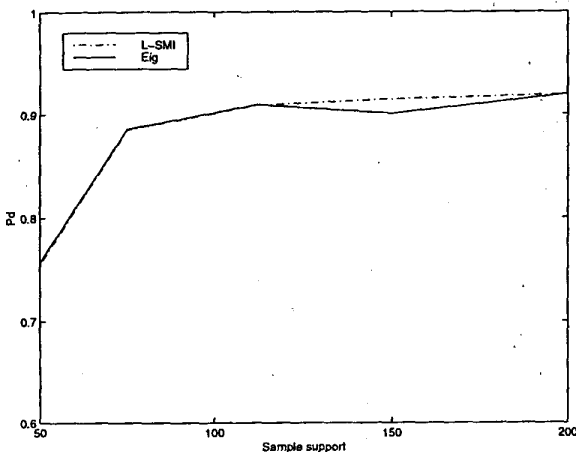


Fig. 11. Performance as function of sample support.

are shown in Fig. 9. The figure demonstrates that L-SMI and the eigencanceler produce high values of the CSNR. Detection probability curves are shown in Fig. 10 for a constant false-alarm rate of  $10^{-5}$ . The performance of the radar as a function of sample support is investigated in Fig. 11. The detection probability is plotted as a function of the sample support  $K$ , for a fixed  $\text{SNR} = 22$  dB. It can be observed that performance improves as a function of sample support up to  $K = 75 \cong 4r$ ; it remains stable thereafter. The performance of L-SMI and eigencanceler are similar.

The range-ambiguous clutter map is shown in Fig. 7. The clutter has Doppler returns in approximately 12 out of the 64 Doppler bins used. The J-hook shape of the clutter ridge is apparent in the figure. The post-processing clutter maps for L-SMI and the eigencanceler are provided in Figs. 12 and 13, respectively. The two figures show that the

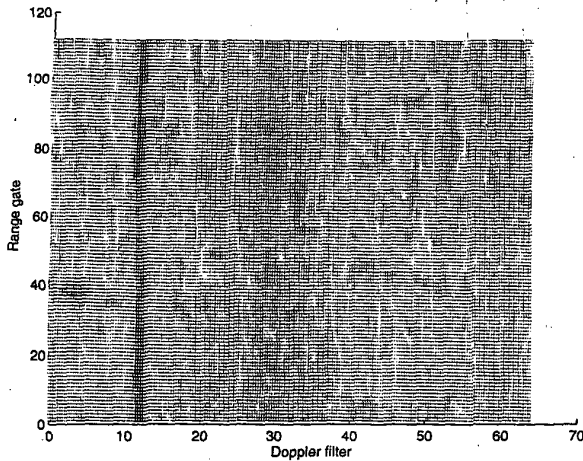


Fig. 12. Post-processing clutter using L-SMI.

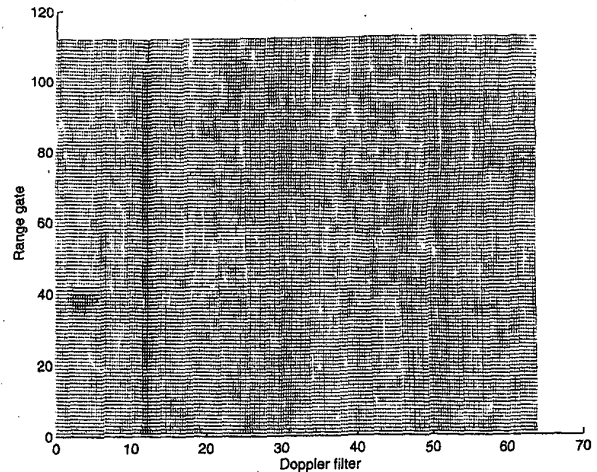


Fig. 13. Post-processing clutter using eigencanceler.

near-range clutter masking the target has been rejected and the target is now evident.

Finally, the effect of the target presence in the training data is investigated for the L-SMI and the eigencanceler. A target with  $\text{SNR} = 10$  dB was included in the training set used to obtain the sample covariance matrix as in (23). The probability density functions of the CSNR for both methods were obtained by averaging 10,000 Monte-Carlo runs. The simulated CSNR distribution curves with and without the target included are given in Fig. 14. The theoretical CSNR distributions are provided for comparison reasons in Fig. 15. The simulation and theoretical results of the CSNR distributions are shown to be in good agreement.

## V. CONCLUSIONS

This paper discusses the application of STAP techniques to suppress the interference effects of ground clutter in HPRF radars. It is shown that adaptive processing for HPRF radars is characterized by reduced sample support. Reduced-rank methods are necessary to overcome this problem. Four STAP methods are compared in this work: P-SMI, L-SMI, eigencanceler, and element-space post-Doppler. The four techniques are compared through the performance measures of CSNR and probability of detection. It is shown that the eigencanceler and L-SMI perform similarly. P-SMI does not perform satisfactorily. The performance of the element-space

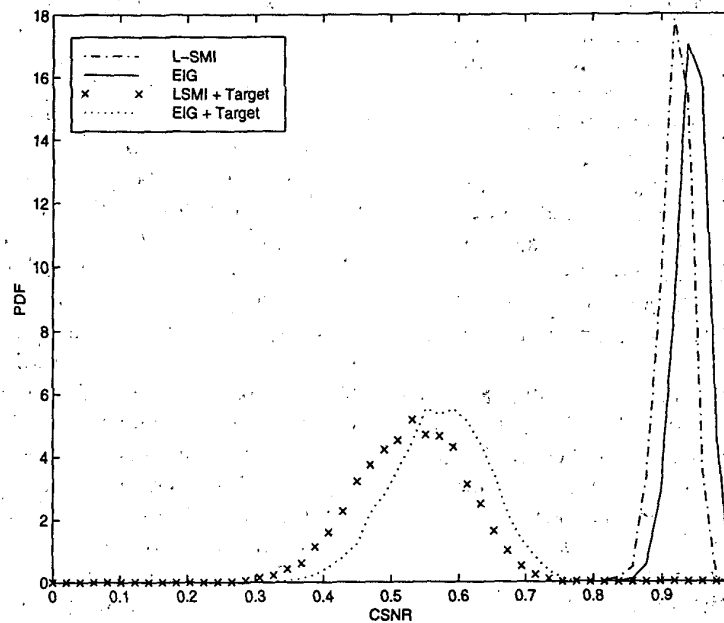


Fig. 14. Simulation PDF of CSNR with and without desired signal present.

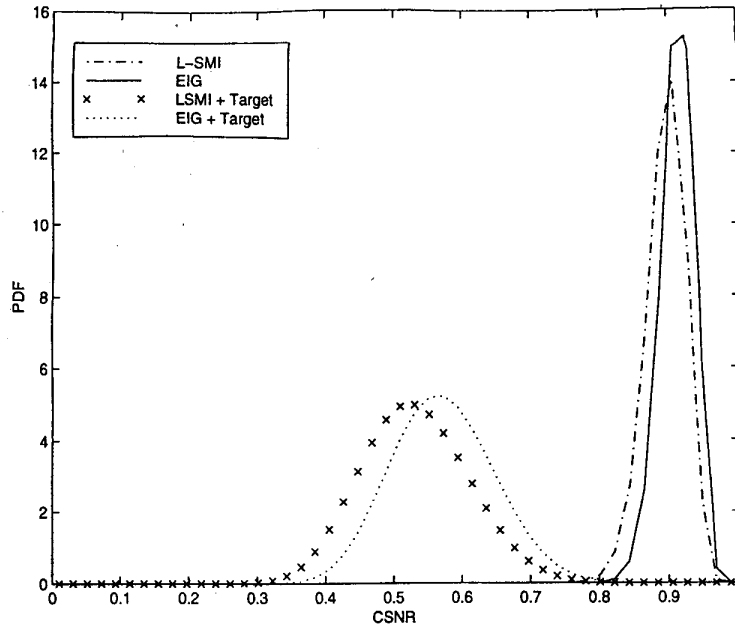


Fig. 15. Theoretical PDF of CSNR with and without desired signal present.

post-Doppler method shows that only spatial degrees of freedom are not sufficient to cancel the clutter in this case. Although the size of the secondary data used to estimate the sample covariance matrix exceeds the dimensionality of the system in this case, the output CSNR was mediocre.

#### REFERENCES

- [1] Brennan, L. E., and Reed, I. S. (1973) Theory of adaptive radar. *IEEE Transactions on Aerospace and Electronic Systems*, AES-9 (Mar. 1973), 237–252.
- [2] Wang, H., and Cai, L. (1994) On adaptive spatial-temporal processing for airborne surveillance radar systems. *IEEE Transactions on Aerospace and Electronic Systems*, 30 (July 1994), 660–668.
- [3] Barile, E., Fante, R., and Torres, J. (1992) Some limitations on the effectiveness of airborne adaptive radar. *IEEE Transactions on Aerospace and Electronic Systems*, 28 (Oct. 1992), 1015–1031.
- [4] Ward, J. (1994) Space-time adaptive processing for airborne radar. Technical report 1015, Lincoln Laboratory, M.I.T., Lexington, MA, Dec. 1994.
- [5] Brennan, L. E., Piwinski, D. J., and Staudaher, F. M. (1993) Comparison of space-time adaptive processing approaches using experimental airborne radar data. In *Proceedings of the 1993 IEEE National Radar Conference*, 1993, 176–181.
- [6] Dilsavor, R. L., and Moses, R. L. (1993) Analysis of modified SMI method for adaptive array weight control. *IEEE Transactions on Signal Processing*, 41 (Feb. 1993), 417–422.
- [7] Carlson, B. D. (1988) Covariance matrix errors and diagonal loading in adaptive arrays. *IEEE Transactions on Aerospace and Electronic Systems*, 24 (July 1988), 397–401.
- [8] Abramovich, Y. I. (1981) Controlled method for adaptive optimization of filters using the criterion of maximum signal to noise ratio. *Journal of Communication Technology and Electronics*, 3 (1981), 87–95.
- [9] Cheremisin, O. P. (1982) Efficiency of an adaptive algorithm with regularization of the sampled correlation matrix. *Journal of Communication Technology and Electronics*, 2 (1982), 69–77.
- [10] Haimovich, A. M. (1996) The eigencanceler: Adaptive radar by eigenanalysis methods. *IEEE Transactions on Aerospace and Electronic Systems*, 32 (Apr. 1996), 532–542.
- [11] Kirsteins, I. P., and Tufts, D. W. (1994) Adaptive detection using low rank approximation to data matrix. *IEEE Transactions on Aerospace and Electronic Systems*, 30 (Jan. 1994), 55–67.
- [12] Chang, L., and Yeh, C. (1992) Performance of DMI and eigenspace-based beamformers. *IEEE Transactions on Antenna and Propagation*, 40 (Nov. 1992), 1336–1347.
- [13] Landau, H. J., and Pollak, H. O. (1962) Prolate spheroidal wave functions Fourier analysis and uncertainty—III: The dimension of the space of essentially time and band-limited signals. *The Bell System Technical Journal* (July 1962), 1295–1336.
- [14] Haimovich, A. M., and Berin, M. (1997) Eigenanalysis-based space-time adaptive radar: Performance analysis. *IEEE Transactions on Aerospace and Electronic Systems*, 33 (Oct. 1997), 1170–1179.

- [15] Reed, I. S., et al. (1974)  
Rapid convergence rates in adaptive arrays.  
*IEEE Transactions on Aerospace and Electronic Systems*,  
**AES-10** (Nov. 1974), 853–863.
- [16] Haykin, S. (1996)  
*Adaptive Filter Theory* (3rd ed.).  
Englewood Cliffs, NJ: Prentice Hall, 1996.
- [17] Haimovich, A. (1996)  
Asymptotic distribution of the conditioned signal-to-noise  
ratio in an eigenanalysis-based adaptive array.  
*IEEE Transactions on Aerospace and Electronic Systems*,  
**33** (July 1996), 988–996.
- [18] Hudson, J. E. (1981)  
*Adaptive Array Principles*.  
London: Peter Peregrinus, 1981.
- [19] Monzingo, R. A., and Miller, T. W. (1980)  
*Introduction to Adaptive Arrays*.  
New York: Wiley, 1980.
- [20] Abramowitz, M., and Stegun, I. A. (1972)  
*Handbook of Mathematical Functions*.  
Washington, DC: National Bureau of Standards, 1972,  
tenth printing.



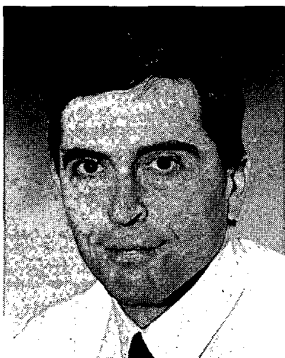
**Tareq F. Ayoub** received the B.S. and M.S. degrees in electrical engineering from Manhattan College, Riverdale, NY, in 1992 and 1993, respectively. He received his Ph.D. degree in electrical engineering from the New Jersey Institute of Technology, Newark, NJ, in 1998.

He currently is a member of the technical staff at AT&T.



**Mark L. Pugh** was born in Utica, NY on April 17, 1960. He received the B.S.E.E. degree from Clarkson University, Potsdam, NY, in 1982 and the M.S.E.E. degree from Syracuse University, Syracuse, NY, in 1985.

In 1982 he joined the Aerospace Electronics Systems Division of General Electric Company in Utica, NY where he developed electronic counter measure (ECM) systems for airborne radar applications. From 1985 to 1989 he was a Member of the Research Staff at the Riverside Research Institute in Rome, NY where he managed midcourse radar data collection experiments and performed radar system analysis for the strategic Defense Initiative. From 1989 to 1999 he was the Program Manager for Advanced Radar Systems at the Air Force Research Laboratory in Rome, NY where he led the development of advanced technologies for airborne and space-based surveillance radar systems. Since March of 1999 he has been the Program Manager for Information Exploitation and Fusion in the Air Force Research Laboratory's Information Directorate.



**Alexander M. Haimovich** (M'89—SM'97) received the B.Sc. degree in electrical engineering from the Technion Institute of Technology, Haifa, Israel in 1977. He received the M.Sc. degree in electrical engineering from Drexel University, Philadelphia, PA in 1983, and the Ph.D. degree in systems from the University of Pennsylvania, Philadelphia, in 1989.

From 1983 to 1987 he was a Senior Engineer with American Electronic Laboratories in Lansdale in Lansdale, PA. From 1987 to 1989 he was an Assistant Professor at the New Jersey Institute of Technology. He was a Senior Staff Consultant at American Electronic Laboratories from 1989 to 1990. From 1990 to 1992 he was Chief Scientist at JJM Systems, Warminster, PA. He is currently Associate Professor of Electrical and Computer Engineering at the New Jersey Institute of Technology. His research interests include adaptive array processing for radar and wireless communications.